Shock induced atomisation of a liquid metal droplet

Shubham Sharma[1], Navin Kumar Chandra[1], Aloke Kumar[1] and Saptarshi Basu[1,2*]

[1] Department of Mechanical Engineering, Indian Institute of Science, Bangalore – 560012, India

[2] Interdisciplinary Center for Energy Research (ICER), Indian Institute of Science,

Bangalore – 560012, India

Supplementary Table

Weber number	Ga-A	Ga-N	Wa-A	Difference with Ga-N in percentage	
				Ga-A	Wa-A
1500	1432	1500	1513	4.5	0.87
1700	1796	1609	1520	-11.6	-5.5
2000	1993	1968	2096	-1.27	6.5
3300	3619	3209	3314	-12.77	3.3
6100	6599	6189	5428	-6.2	-12.3

Table S1: Variation in Weber number values for different cases considered in droplet deformations.

We	Breakup induction time (t_{in})			Cross stream deformation at first breakup ($D_{m_{in}}/D_{mi}$)		
	Ga A	Ga N	Wa A	Ga A	Ga N	Wa A
1500	0.54	0.58	0.73	1.34	1.58	1.57
1700	0.61	0.57	0.73	1.37	1.51	1.57
2000	0.64	0.49	0.66	1.65	1.51	1.48
3300	0.58	0.65	0.57	1.30	1.43	1.62
6100	0.60	0.62	0.52	1.25	1.49	1.57
2400	0.67	0.57	0.56	1.50	1.75	1.38
Average	0.60	0.58	0.63	1.40	1.55	1.53
Standard Deviation	0.03	0.05	0.08	0.13	0.10	0.08

Table S2: Breakup induction time and cross stream droplet deformation at that instant for different Weber number (We) values.

Charging Voltage (kV)	M_s at $(r = r_d)$	$P_{g,max}$ (bar)	$U_{g,max}$ (m/s)	$\rho_{g,max}$ (kg/m^3)
5	1.18	1.46	95	1.54
6	1.29	1.76	144	1.75
6.75	1.34	1.91	167	1.85
7.5	1.42	2.21	207	2.04
9	1.57	2.69	265	2.32
11	1.71	3.26	324	2.61

Table S3: Peak values of fluid properties at droplet location. Adapted from, Chandra et al. 2023.

Supplementary Figures

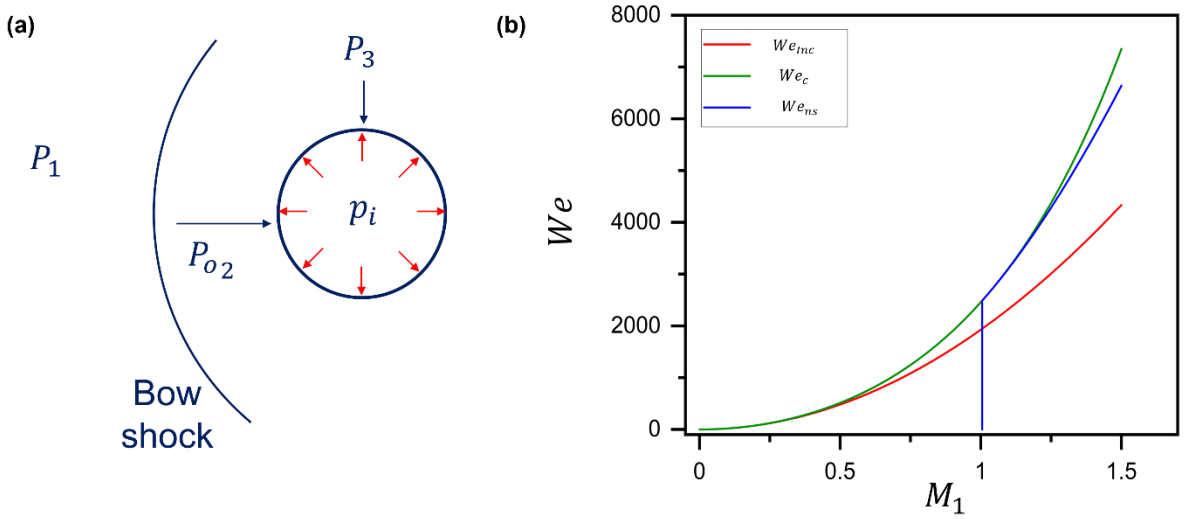

Figure S1: (a) Schematic diagram showing bow shock formation due to supersonic flow interaction with the Galinstan droplet in air. (b) Representation of various Weber number definitions variation with shock-induced flow Mach numbers ($M_1 = V_i/a$). Here, the Incompressible flow-based Weber number is represented as $\left(We_{inc} = \frac{\rho_g V_i^2 D_o}{\sigma}\right)$, Compressible flow-based Weber number is represented as $\left(\frac{2(P_{o_1} - P_3)}{\sigma/D_o}\right)$ and Compressible flow with normal shock-based Weber number is represented as $\left(\frac{2(P_{o_2} - P_3)}{\sigma/D_o}\right)$. Note that We_c the definition is equivalent to We_{inc} for $M_1 < 0.5$. In the studied range of induced flow Mach numbers We_{inc} and We_{ns} are equivalent as a weak bow shock formed in present case.

Transient charecterstics of present shock tube:

A short summary of transient charecterstics of flow proile in present shock tube is presented here. For a detailed discussion reader is encouraged to follow our previous works (Chandra et al. 2023, Sharma et al. 2021). The shock wave produced in the current experimental arrangement closely resembles a planar wave because of the rectangular confinement of the shock tube channel. Nevertheless, once the shock wave exits the shock tube, it naturally transitions from a planar wave to a spherical wave. However, due to the close proximity of the droplet location to the open end of the shock tube, we can continue using the assumption of a planar shock front in this specific region. As a result, we adopt the analytical solution proposed by Bach & Lee (1970) and apply numerical methods to solve it, considering the present geometry and the assumption of a planar shock front.

To verify the validity of this hypothesis under the current conditions, it is not feasible to conduct direct experimental measurements of gas velocity and pressure due to limitations in our available experimental facility. Nonetheless, we can determine the shock arrival time (t_{arr}) through experimentation. The time t_{arr} represents the duration taken by the shock front to travel from the blast position (r = 0) to the droplet location (r = r_d = 33.5 cm). The estimation of t_{arr} is achieved by analyzing images obtained from a global observation imaging setup. The initiation of the blast event is detected through a saturated image captured by the camera, caused by

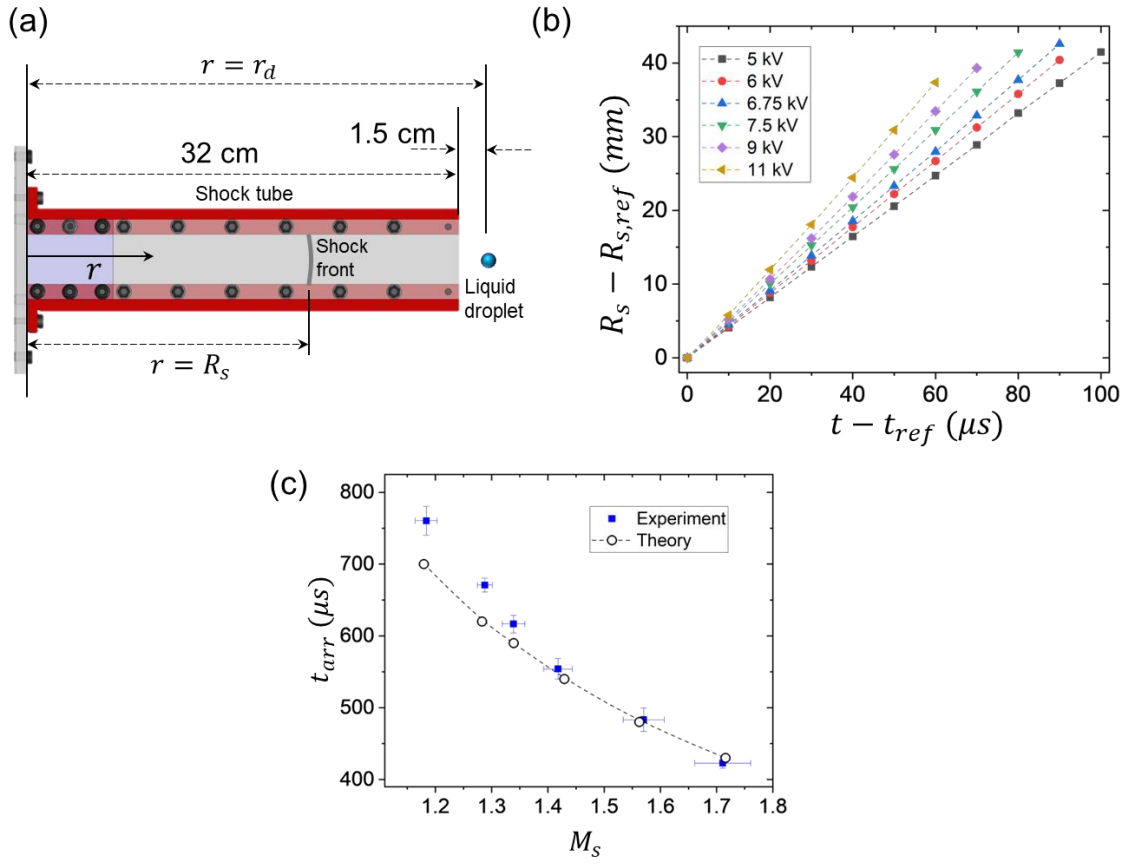

Figure S2: Transient flow charecterstics of shock tube. (a) Geometery of shock tube. (b) Time variation of shock front position, corresponding to different values of capacitor charging voltage. (c) Shock arrival time tarr obtained from experiments and theory for different values of M_s. Note that the reported Ms corresponds to its value when the shock front is at the droplet location. Shock Mach number and peak fluid properties magnitude corresponding to each charging voltage is shown in supplementary table S3. Adapted with permission from Chandra et al. 2023.

a powerful flash of light during the wire blast. Subsequently, the shadowgraphic images directly capture the shock front as it reaches the droplet location. By utilizing these two frames,

the experimental value of t_{arr} can be determined. The theory aligns remarkably well with the experimental results, as illustrated in figure 12. The maximum error observed is approximately 50μs, which is negligible given the inherent uncertainty of ±25μs in determining t_{arr} experimentally, owing to the 40,000 fps recording rate. It is important to note that the error bars in figure 12 do not consider this uncertainty. Instead, they represent the standard deviation of t_{arr} and M_s obtained from ten different experimental runs. The excellent agreement in predicting t_{arr} strongly supports the applicability of Bach and Lee's theory (1970) to our present setup, at least within the time duration where the shock front can be reasonably approximated as planar.

In the following discussion, we will explore the temporal decay of gas flow properties at the droplet location. Figure ** shows that the Mach number (M_s) does not experience significant decay as the shock wave passes near the drople. However, this does not guarantee a similar pattern for the temporal variation of gas density, velocity, and pressure at any specific point. The behavior of these fluid properties depends on two factors: the Mach number of the shock front advancing ahead of the desired location and the distance between the desired location and the shock front. As time progresses, both of these factors diminish, resulting in an exponential decline of fluid properties at a fixed location behind the moving shock wave. The transient decay of the Mach number of the shock front after it has passed the droplet location is illustrated in figure 13(a). We denote the absolute pressure, velocity, and density of the gas

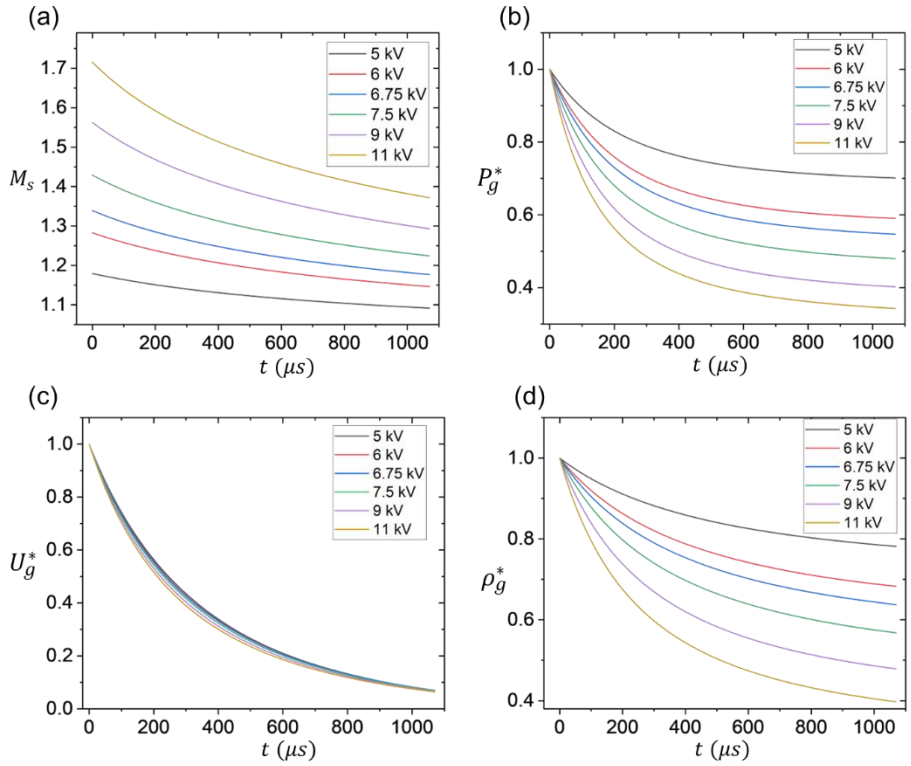

Figure S3: (a) Transient evolution of shock Mach number after the passage of the shock front from the droplet location. Time t = 0 corresponds to moment of droplet–shock wave interaction. Transient evolution of (b) absolute pressure, (c) velocity and (d) density of the gas phase at the droplet location.

phase at any location r and time t as $P_g(r,t)$, $U_g(r,t)$, and $\rho_g(r,t)$, respectively. Figures 13(b–d) depict the theoretically estimated transient evolution of P_g, U_g, and ρ_g following the passage of the shock front at the droplet location. In these figures, the fluid properties are normalized by their maximum values and defined as follows:

$$P_g^* = \frac{P_g(r=r_d,t)}{P_{g,max}}; \qquad U_g^* = \frac{U_g(r=r_d,t)}{U_{g,max}}; \qquad \rho_g^* = \frac{\rho_g(r=r_d,t)}{\rho_{g,max}};$$

In this study, the moment when the shock wave interacts with the droplet is denoted as t = 0. At this point, the gas pressure, velocity, and density reach their maximum values at the droplet's location. Figure 13 illustrates that the gas phase properties decay rapidly over time in contrast to the standard shock tube configuration, where constant fluid properties can be maintained for an extended period. When comparing our results with existing literature, it is crucial to take into account these transient properties inherent to our experimental setup.

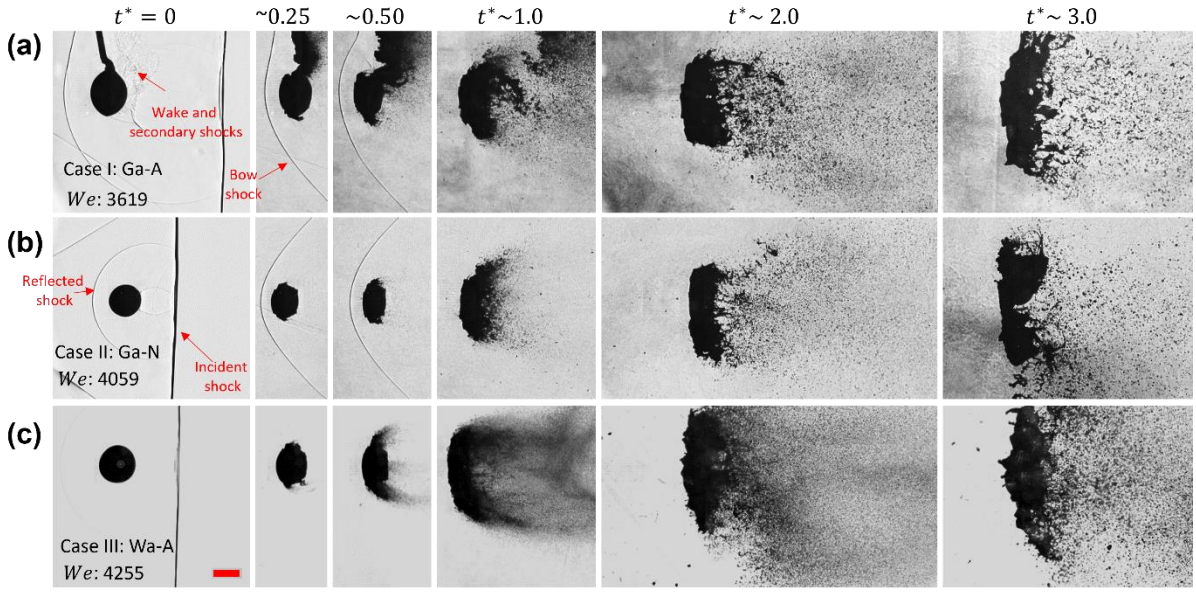

Figure S4: Global view of atomisation dynamics. (a) Case I: Galinstan-air system (Ga-A) with $We = 3619$, (b) Case II: Galinstan-nitrogen system (Ga-N) with $We = 4059$, (c) Case III: Water-air system (Wa-A) with $We = 4255$. Scale bar equal 2 mm.

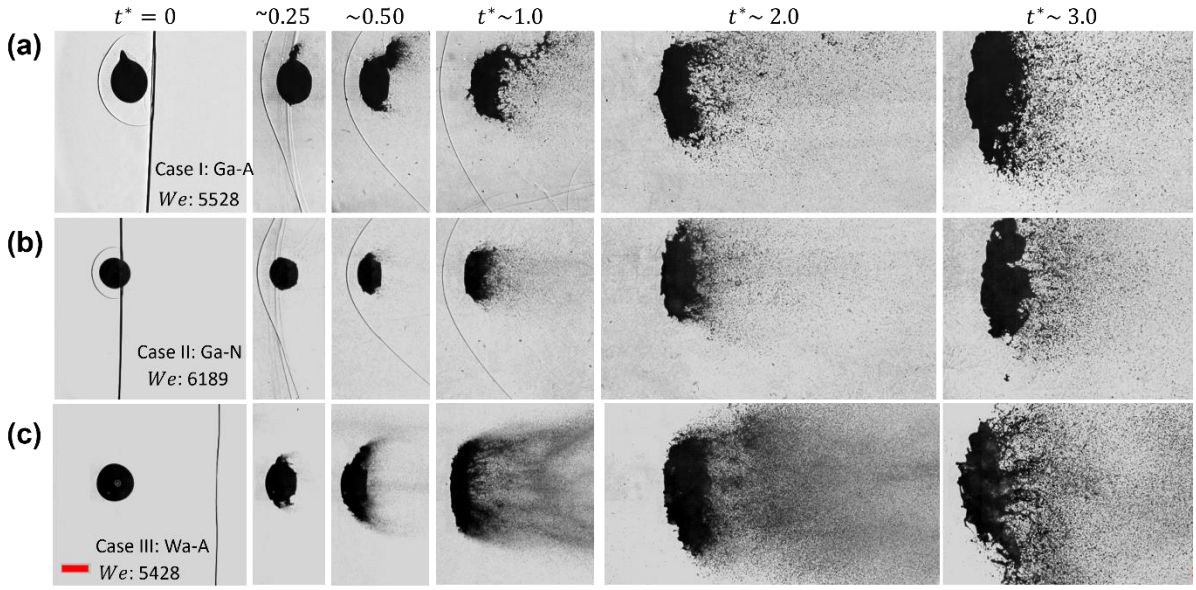

Figure S5: Global view of atomisation dynamics. (a) Case I: Galinstan-air system (Ga-A) with $We = 5528$, (b) Case II: Galinstan-nitrogen system (Ga-N) with $We = 6189$, (c) Case III: Water-air system (Wa-A) with $We = 5428$. Scale bar equal 2 mm.

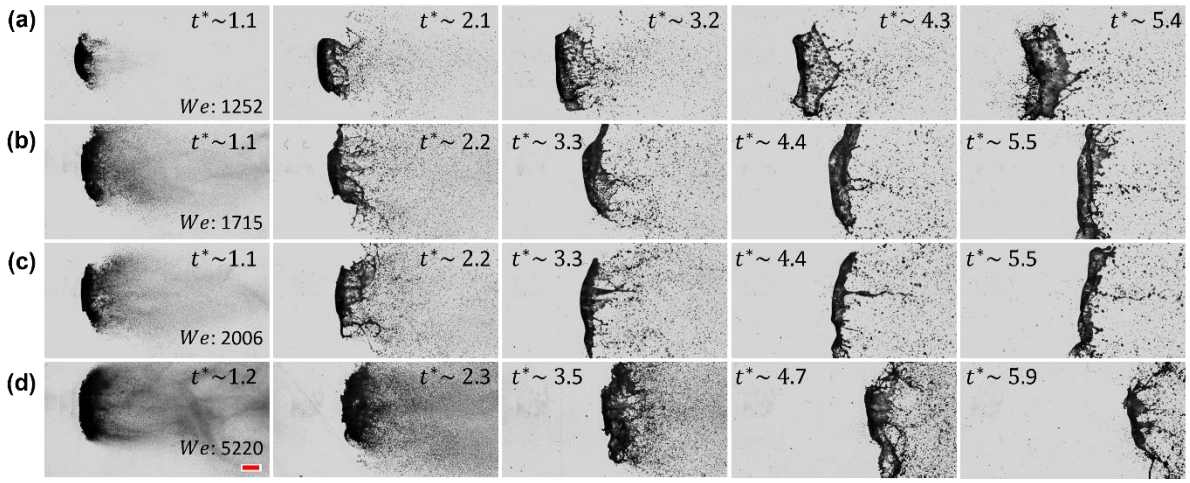

Figure S6: Evolution dynamics of an atomising Water droplet in air for different Weber number (We) values. (a) Water-air $We = 1252$, (b) Water-air $We = 1715$, (c) Water-air $We = 2006$, and (d) Water-air $We = 5220$. Scale bar equal 2 mm.

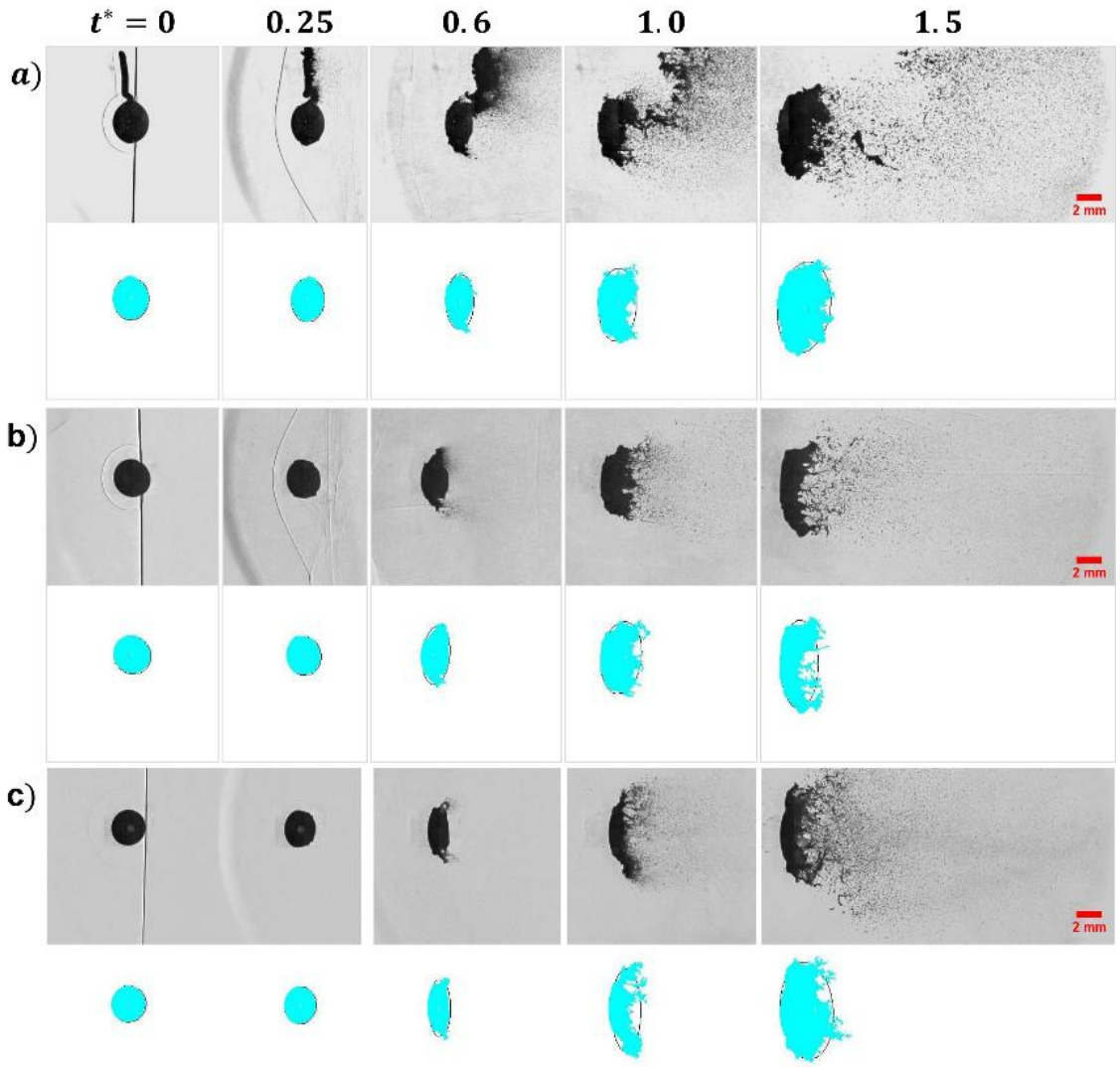

Figure S7: Measurement of cross stream deformation at $We \sim 1700$ for different time isntaces. (a) Galinstan-air (b) Galinstan-nitrogen (c) Water-air.

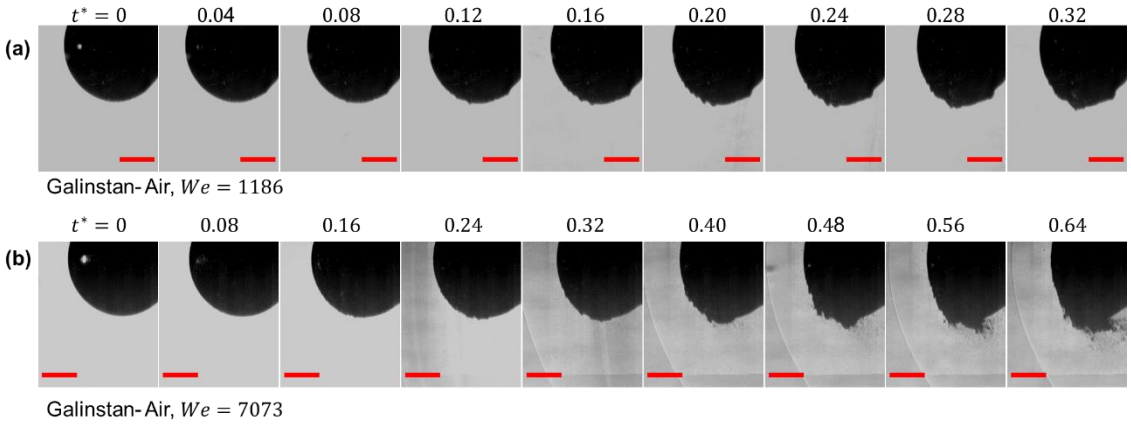

Figure S8: Time evolution of KH waves on droplet surface at (a) $We = 1186$ (b) $We = 7073$. Scale bar equals to 1 mm.